NASA TECHNICAL MEMORANDUM

NASA TM X-67854

NASA TM X-67854

WIND TUNNEL TESTS OF A WING-INSTALLED MODEL VTOL LIFT FAN WITH COAXIAL DRIVE TURBINE

by S. Lieblein, J. A. Yuska, and J. H. Diedrich
Lewis Research Center
Cleveland, Ohio

TECHNICAL PAPER proposed for presentation at
Seventh Propulsion Joint Specialists Conference sponsored by
the American Institute of Aeronautics and Astronautics
Salt Lake City, Utah, June 14-18, 1971

WIND TUNNEL TESTS OF A WING-INSTALLED MODEL VTOL LIFT FAN WITH COAXIAL DRIVE TURBINE

by S. Lieblein,* J. A. Yuska,** and J. H. Diedrich***

National Aeronautics and Space Administration
Lewis Research Center
Cleveland, Ohio

E-6359

ABSTRACT

This paper presents a summary of principal results obtained from crossflow tests of a 15-in.-diameter lift fan installed in a wing in the NASA, Lewis Research Center, 9- by 15-Foot V/STOL Wind Tunnel. The basic objective of the investigation was to determine lift fan behavior in the crossflow environment and to define the principal factors affecting fan performance. The fan stage was designed for a pressure ratio of 1.28 at a corrected tip speed of 980 ft/sec. The unique feature of the fan is a compact drive turbine coaxially mounted within the hub section of the fan. This arrangement provided for coaxial exhaust streams. Tests were run with and without exit louvers over a wide range of tunnel air speeds, fan speeds, and wing angle of attack. The results presented herein provide a comparatively complete picture of the basic features of the internal flow in a lift fan in crossflow. In addition to presenting data on the internal reactions to inflow distortion, the paper points to the added importance of back pressure effects in influencing fan performance. In this particular fan, flow separation on the inlet bellmouth did not appear to be a serious problem for crossflow operation.

---

*Chief, VTOL Propulsion Branch.

**Project Engineer, VTOL Performance Section.

***Head, VTOL Performance Section.

INTRODUCTION

The high-bypass-ratio lift fan is currently a prime candidate for the lift propulsion system for VTOL transport aircraft. Numerous studies (e.g., refs. 1 to 6) have indicated the potential feasibility of lift fan VTOL aircraft, while many experimental investigations have shown acceptable performance characteristics for fan aircraft configurations (e.g., refs. 7 to 13). A recent review of lift fan propulsion for civil V/STOL transports is contained in Ref. 14.

A principal concern with lift fan aircraft is the induced effects on overall aircraft aerodynamics generated by the large masses of air that are set in motion by the fans. These induced effects are felt while the aircraft is near the ground at takeoff and landing (in-ground effect), and while the aircraft is proceeding from the vertical to the horizontal flight mode (crossflow effect). Induced lift, drag, and pitching moments of significant magnitude and directional variation have been observed for various aircraft/propulsion configurations.

From the propulsion point of view, a corollary question is the influence of the crossflow and ground environment on the basic performance of the fan. Of particular concern is the effect of flow distortions and interactions that operate on both the inlet and outlet flows of the fan during transition (ref. 15). Such crossflow-induced interactions can have significant effects on fan operating point, thrust level, and efficiency.

The potential adverse effects of the crossflow component on the flow into the fan inlet have been well documented in a number of studies (e.g., refs. 16 to 33). These investigations have revealed the presence of boundary layer separation on the inlet bellmouth surfaces and circumferential variations in flow components at the face of the fan rotor under crossflow conditions. However, little experimental or analytical information has appeared on possible outlet flow interactions or on the detailed nature of the response of a fan stage to inlet and outlet distortions during transition.

This paper presents a summary of the principal results obtained from crossflow tests of a 15-in.-diameter lift fan installed in a wing in the NASA, Lewis Research Center, 9- by 15-Foot V/STOL Wind Tunnel. The fan

stage was designed for a pressure ratio of 1.28 at a rotor corrected tip speed of 980 ft/sec. The unique feature of this fan is a compact, high-pressure-air drive turbine which is coaxially mounted within the hub section of the fan. This arrangement provided for coaxial exhaust streams. Extensive internal instrumentation was included in addition to load cell measurement of overall wing forces and fan-assembly axial force.

The basic objective of the investigation was to determine lift fan behavior in the crossflow environment and to define the principal factors affecting fan performance. The experiments were conducted over a wide range of tunnel air velocity (up to 170 mph), wing angle of attack ($\pm 15^{\circ}$), and fan tip speed (70 to 110 percent). Tests were run with and without exit louvers and with various modifications to the fan inlet and outlet geometry.

The discussion starts with representative variations with crossflow velocity of total-assembly and fan-stage gross thrust, followed by data on stage outlet total pressure and flow rate. The causes for the observed trends are then explored through examination of the flow in the inlet bellmouth and across the rotor and stator blade rows. Fan back pressure variations are then presented, and the paper concludes with plots of performance maps for lift fan application.

APPARATUS

Test Setup

The 15-in.-diameter model lift fan was installed in a two-dimensional wing and tested in the NASA Lewis Research Center 9- by 15-Foot V/STOL test section, as shown in Fig. 1. The wing spanned the 9-ft height of the test section and had a 4.5 ft chord. The wing has a constant airfoil section with a maximum thickness ratio of 17 percent (modified NACA 65_3A(218)-217 section). The model lift fan was installed at midspan with its axis located at the 40 percent chord position. Remote actuation of the wing assembly was provided over a range of angle of attack from -15° to $+15^{\circ}$. However, during static tests (no crossflow), the wing was located with its

chord perpendicular to the axis of the test section (-90^{o}) to eliminate flow recirculation effects. Descriptive details of the test tunnel are given in Ref. 34.

A cross section of the lift fan assembly is shown in Fig. 2 to illustrate the major aerodynamic and mechanical features of the test model. The fan rotor was driven by a compact two-stage supersonic turbine located in the hub section of the assembly. High-pressure air to drive the turbine was supplied through six equally-spaced 12-percent-thick struts spanning the fan passage. These struts also served as the structural support for the inner components of the assembly. The outer casing of the fan was attached to the wing by a balance system consisting of three load cells equally spaced on a 22.5-in.-diameter circle.

The rotor tip leading edge was located 2.4 in. axially from the peak height of the forward point of the inlet bellmouth. This provided for a ratio of inlet depth to rotor tip diameter of 0.16. Two 0.060-in.-diameter damper wires were located on the rotor blades at 60 percent of the passage height from the hub to reduce blade vibration and prevent blade flutter in crossflow. The axial spacing between rotor and stator blades was approximately 0.75 in. Four louver vanes for aft flow deflection were attached to the wing with remote actuation from a vane chord position of -2.5^{o} to 40^{o} from the fan axis.

Design Characteristics

The inlet bellmouth was designed according to the method described in Ref. 35 to avoid velocity peaks on the outer shroud during static (no crossflow) operation. The exit louvers were 8 percent thick airfoil sections (NACA 63-series, 0.6 lift coefficient) with a solidity of 1.2 and aspect ratio of 3.3. The fan stage was designed according to the general approach of Ref. 36. Design axial thrust for the fan stage was 810 lb and design power input was 580 horsepower at ambient conditions of 2116 lb/ft^2 and 80^{o} F. Some specific design characteristics of the fan stage are listed in Table I.

TABLE I. - LIFT FAN DESIGN CHARACTERISTICS

Overall pressure ratio	1.28
Corrected tip speed	980 ft/sec
Corrected weight flow	39.8 lb/sec
Inlet axial Mach number	0.60
Exit static pressure	2116 lb/ft^2
Rotor Blade (double circular arc airfoil section)	
Number of blades	35
Tip diameter	15.2 in.
Aspect ratio	2.6
Hub-tip ratio	0.463
Solidity (tip)	1.25
Stator Blade (NACA 65 series airfoil section)	
Number of blades	36
Aspect ratio	3.0
Solidity (tip)	1.0

The drive turbine was scaled from a previous NASA design reported in Refs. 37 and 38. The turbine had a mean diameter of 5.4 in. Scaling of the reference turbine was calculated to develop 685 horsepower at 105 percent of fan design speed. Principal drive turbine design characteristics (at 105 percent fan design speed) are summarized in Table II.

TABLE II. - DRIVE TURBINE DESIGN CHARACTERISTICS

Inlet pressure	1000 $lb/in.^2$
Inlet temperature	630° R
Actual weight flow	9.72 lb/sec
Actual speed	16,000 rpm
Overall total efficiency	0.534
Specific work	49.9 Btu/lb

Instrumentation

The major features of the fan internal instrumentation are shown in Fig. 2. For the inlet bellmouth, static taps were located at eight circumferential positions on the outer shroud. For each of these positions, eight taps were spaced along the surface from 0.25 in. to 3.6 in. from the rotor inlet plane. Three 0.25-in.-long wall rakes, each with four total pressure probes, were placed at three circumferential positions on the forward half of the inlet (0^{o}, -55^{o}, and $+55^{o}$) and approximately 0.5 in. forward of the rotor leading edge.

At the rotor exit, six fixed-position angle rakes were equally spaced around the circumference to measure flow angle and total pressure at three radial positions. Six equally-spaced stators each carried six total pressure probes. An additional six stators were each instrumented with three total temperature probes. Static taps were located at six equally-spaced positions on the hub and tip surfaces in the measuring plane of the total pressure probes.

At the duct exit, six fixed-position rakes equally spaced around the circumference (in mid-passage of struts) were used to measure flow angle at three radial positions and total pressure at five radial positions. Static taps were located at six equally-spaced positions on the hub and tip surfaces in the measuring plane of the total pressure probes.

The turbine exit duct was instrumented at two circumferential locations to measure flow angle at one radial position, total pressure at five radial positions, and total temperature at two radial positions. Two equally-spaced static taps were located on the turbine exit inner and outer wall surfaces. Turbine air weight flow was measured by a calibrated flat plate orifice, while temperature and pressure of the turbine drive air were measured in the turbine inlet plenum. Base static pressures were measured on the ring between the fan and turbine flow passages and on the centerbody surface of the turbine.

PERFORMANCE VARIATIONS

The overall crossflow performance of the fan assembly, consisting of the

fan stage, drive turbine, and inlet bellmouth, is shown in Fig. 3. Data are presented at rotor corrected design tip speed (980 ft/sec) for total gross thrust and drive-turbine power output, both expressed as a ratio of the frontal area of the fan (rotor tip diameter = 15.2 in.). The total thrust was computed as the sum of the fan discharge and turbine discharge thrusts and the net force on the inner base of the turbine. Both fan thrust and power input tend to decrease with increasing crossflow velocity. Angle of attack starts to become a variable at the high values of crossflow velocity.

At a crossflow velocity of 240 ft/sec (164 mph) and zero-degree wing angle of attack, the total thrust decreased by around 12.5 percent compared to the zero crossflow value. At zero angle of attack, ratios of total thrust to horsepower input varied from 1.62 lb/hp at zero crossflow to 1.53 lb/hp at 240 ft/sec.

Fan Thrust

The thrust variation of the fan stage alone is shown in Fig. 4 for 70 and 100 percent design speed conditions. At design speed, as in the case of the total thrust, the fan thrust decreases with increasing crossflow velocity. At 70 percent speed, however, thrust tends to rise slightly, except for the high angle of attack configuration. In all cases, increased wing angle of attack at high crossflow velocities resulted in a reduction of fan thrust. At zero angle of attack and design speed, the decrease in fan stage thrust at 240 ft/sec is around 11 percent compared to a decrease of around 12.5 percent for the total thrust (fig. 3). Thus, the behavior of the fan stage thrust can be taken as a valid measure of the variation of the total thrust.

Also shown for comparison in Fig. 4 is the variation in ideal gross thrust computed assuming complete recovery of the momentum of the crossflow entering the fan (i.e., as crossflow velocity increases, ambient total pressure increases, inlet pressure losses are zero, total pressure ratio across the stage remains constant, and outlet static pressure is the ambient value). Under this assumption, ideal fan thrust increases with increasing crossflow velocity. A significant deviation from ideal fan thrust is observed, especially at the higher tip speed.

The influence of exit louvers on the gross thrust of the fan stage is shown in Fig. 5 for two tip speed conditions. Since gross thrust is computed from measured flow conditions at the exit of the fan duct, the variations in gross thrust represent the back pressure effect of the louvers on the fan. At design speed, variations in louver angle had a significant effect on gross thrust only at zero or low crossflow velocities. No discernable effect of louver position appeared at the low tip speed.

The acceptability of the performance variations exhibited in Figs. 3 to 5 in an actual aircraft application will depend on a number of factors. Obviously, since wing lift increases with forward speed during transition, less vertical lift will be required from the fans. However, if exit louvering is utilized for thrust vectoring (for horizontal acceleration and deceleration, or attitude control), a high value of gross thrust may be required over the entire transition flight range because of the cosine effect and thrust losses across the louvers. Thus, the specific requirement for fan gross thrust will depend on the particular aircraft configuration and the transition flight procedure used.

In addition to the question of adequate available thrust, the rather significant departure of the actual thrust from the ideal variation warrants attention. Such deviation represents a form of inefficiency which may have some fundamental unfavorable attributes such as excessive fuel consumption or increased noise generation. Thus, it seems desirable to investigate the causes of the indicated thrust fall off in crossflow.

Total Pressure and Weight Flow

Inasmuch as fan gross thrust is determined primarily by outlet total pressure and weight flow rate, it is of interest to examine these variations in crossflow. The variation in ratio of average duct-exit total pressure to ambient static pressure is shown in Fig. 6 for two tip speeds and several wing angle of attack positions. A significant decrease in outlet total pressure is observed at design speed, with only a small fall-off at 70 percent speed. For both speeds, an increase in wing angle of attack resulted in a

reduction in outlet total pressure at high crossflow velocities. The deviation of actual total pressure from the ideal variation is quite pronounced at design tip speed.

The fall-off in outlet total pressure with crossflow velocity also represents a loss in efficiency of fan performance, which would ultimately appear as an increase in specific fuel consumption for the powerplant driving the fan. For example, if fan efficiency were constant, the reduction in stage pressure ratio from 1.25 at zero crossflow velocity to 1.22 at 240 ft/sec at zero angle of attack should result in a reduction in required ratio of input power to fan stage thrust from around 0.77 hp/lb to 0.72 hp/lb. However, the measured ratio at 240 ft/sec was 0.79 hp/lb. This represents an increase in required power of 10 percent, and an increase in specific fuel consumption of about the same amount for the crossflow condition.

The corresponding variation in fan stage flow rate per unit frontal area in crossflow is shown in figure 7. A modest decrease in flow rate with crossflow velocity is obtained at design tip speed. This decrease in flow rate, together with the decrease in outlet total pressure (fig. 6), provides the basis for the marked fall-off in stage thrust with crossflow velocity at design tip speed shown in Fig. 4. At 70 percent design speed, however, there is a slight rise in flow rate over the initial crossflow velocity range. This tends to compensate for the slight decline in outlet total pressure (fig. 6) to produce the essentially constant thrust level found in Fig. 4. The marked effect of increasing angle of attack in reducing fan flow rate at high crossflow velocities is clearly evident at both tip speed levels.

It now remains to investigate the fan internal flow conditions in order to determine the factors which produced the observed trends of weight flow rate and outlet total pressure.

INTERNAL FLOW DISTRIBUTIONS

Fan stage outlet conditions during crossflow are recognized to be affected by the flow conditions at the inlet to the fan rotor, and by the response of the rotor and stator rows to the flow distortions imposed by the inlet flow. Each of these items will now be examined in some detail.

Inlet Bellmouth

Previous inlet experiments and theory have indicated that substantial circumferential and radial variations in velocity and angle will occur during crossflow conditions at the entrance to a fan rotor row that is installed in a shallow inlet bellmouth. The nature of this inlet distortion effect is illustrated in Fig. 8. In crossflow, the inflow velocity is increased over the forward portion of the bellmouth and decreased over the aft portion. At the same time, the incomplete turning of the air results in an advancing/retreating blade motion with respect to the incoming air. These two factors result in a circumferential variation in angle of attack on the rotor blade. Roughly, negative incidence angles might be expected from around 315° to 135°, and positive incidence angles from around 135° to 315°. This form of inlet flow distortion is a potential flow phenomena.

On the surfaces of the inlet bellmouth, the forward portion of the outer shroud and the aft portion of the nosepiece would experience pronounced accelerating and decelerating flows resulting from the surface curvatures. For the practical range of crossflow velocities and inlet bellmouth depths, these surface velocity gradients can lead to local boundary layer separation at the inlet to the rotor. This form of inlet distortion is a viscous flow phenomena.

These two forms of inlet distortion were clearly present in the inlet of the model lift fan tested. Figure 9 shows the measured circumferential variation in static pressure ratio on the outer shroud at a position 0.25 in. upstream of the rotor leading edge. The increase in velocity (decrease in static pressure) in the forward portion ($\theta \sim 0^{\circ}$), and the decrease in velocity (increase in pressure) in the aft portion ($\theta \sim 180^{\circ}$) are quite pronounced as crossflow velocity is increased. The small circumferential variation in static pressure at zero crossflow velocity (static case) is attributed to the nonaxisymmetric nature of the bellmouth geometry (different profiles in spanwise and chordwise planes).

The variation in pressure along the surface of the bellmouth is illustrated in Fig. 10. The data presented were obtained from taps located 10° from the full forward position. Under static conditions, a slight acceleration and then deceleration is observed as the flow approaches the rotor inlet. This

acceleration/deceleration increased rapidly as crossflow velocity increased. Values of surface velocity above the sonic value were attained at crossflow velocities as low as 120 ft/sec.

It was not surprising, therefore, to find evidence of boundary layer separation on the inlet wall rake located at the 0^{o} position. In fact, from the measured total pressure profiles of the three inlet rakes (at 0^{o}, -55^{o}, and $+55^{o}$), and a comparison of weight flow rates determined from duct outlet measurements and correlations for inlet weight flow established from potential flow calculations, it was possible to compute the effective percentage of the inlet annulus area that was blocked by the local buildup in surface boundary layer near the inlet to the rotor. The results are shown in Fig. 11 for 100 percent and 70 percent design speed. Boundary layer blockage showed no tendency to increase until a crossflow velocity of around 140 to 150 ft/sec was reached. Above this velocity, the blockage variation was strongly dependent on the wing angle of attack. The increased boundary layer blockage with increased angle of attack is attributed to the existance of a higher level of velocity and poorer boundary layer condition on the surface of the wing at the start of the fan bellmouth for high angle of attack positions.

Boundary layer separation appeared to be restricted to a relatively small area of the forward portion of the bellmouth, since no separation was evidenced on the rakes at -55^{o} or 55^{o} over the entire range of test variables. Furthermore, the introduction of partial annular vanes near the surface over the forward portion of the bellmouth did not result in any measurable change in fan stage thrust versus crossflow velocity. One vane consisted of an airfoil section extending 180^{o} across the inlet. The second vane was a constant thickness section that was shorter in chord length and circumferential extent (90^{o}). These results were interpreted as indicating that the pressure losses introduced by the presence of the annular vanes essentially counteracted any beneficial effects that resulted from any suppression of the localized boundary layer separation.

The average loss in total pressure involved in the localized separated flow region as sketched in Fig. 11 was less than 1 percent for the worst case (100 percent speed and $+10^{o}$ angle of attack). Thus, the viscous loss effects asso-

ciated with this particular bellmouth design represent a relatively modest inlet loss for the fan stage which is not likely to pose any serious problem for crossflow operation.

Rotor Exit

The second aspect of inlet distortion in crossflow is the circumferential variations in free-stream flow entering the fan stage. Pronounced circumferential variations in both flow angle and total pressure were measured at the outlet of the rotor blade row and at the exit of the fan duct (stator exit). In all cases, these circumferential variations tended to increase in magnitude as crossflow velocity increased. The observed variations were also found to be consistent with corresponding theoretical variations determined from potential flow theory calculations (method of ref. 35).

As indicated earlier in the discussion of Fig. 8, the distortion of the free-stream flow in the inlet bellmouth in crossflow tends to produce a circumferential variation in incidence angle on the fan rotor. These changes in incidence angle should produce circumferential variations in total pressure rise. An example of total pressure measured around the outlet of the rotor at the mid-radius position at design tip speed is given in the upper part of Fig. 12. Reduced total pressure is observed at the 90° position, and increased total pressure is observed at the 270° position as crossflow velocity is increased. For the highest crossflow velocity test condition, the variation from minimum pressure ratio to maximum pressure ratio is quite large (1.13 to 1.35).

Theoretical variations of change in rotor incidence angle as calculated from potential flow theory for the mid-radius position at design conditions are shown on the lower part of Fig. 12. The measured circumferential variation in outlet total pressure shows essentially the same trend as the theoretical change in incidence angle. However, peak variations in total pressure are shifted by around 45° in the direction of fan rotation from the peaks of the change in incidence angle. Circumferential displacement of the flow passing across the rotor is calculated to be of the order of only 15°. Thus, there appears to be a lag between the change in outlet total pressure and the change in incidence angle.

Unlike the theoretical incidence variations, the peak measured total pressure (at 270^{o}) does not continue to rise with increasing crossflow velocity to the same degree that the minimum pressure decreases (at 90^{o}). In fact, only a small increase in peak total pressure is noted as crossflow velocity increases from 70 ft/sec to 240 ft/sec. It may be that some form of local stall condition is reached as incidence angle is increased. As a consequence, the average total pressure over the circumference tends to decrease in crossflow. Specifically, the average rotor outlet total pressure ratio at mid-radius decreases from a value of 1.28 at zero crossflow to a value of 1.22 at 240 ft/sec. This phenomenon of probable local rotor stall due to inlet free-stream distortion may then be one of the principal contributing factors to the observed reduction in overall stage outlet total pressure in crossflow (fig. 6).

An example of flow angle measured at the outlet of the rotor, β_2, at the mid-radius position at design tip speed is given in the upper part of Fig. 13. The test data show maximum angles at around 100^{o} and minimum angles at around 280^{o}. The maximum variation in angle approaches 12^{o} at a crossflow velocity of 240 ft/sec. This angle variation represents the distortion in flow angle entering the stator row (stator inlet distortion).

The lower part of Fig. 13 shows the calculated variation of absolute flow angle at the inlet to the rotor, β_1, at mid-radius as obtained from potential flow theory. The form of the theoretical inlet variation is strikingly similar to the measured outlet variation, although the magnitude of angle change is substantially greater (30^{o} difference for theory vs 12^{o} for data). This difference in magnitude may be the result of the contributing effect of the circumferential variation of rotor pressure rise. In general, for fixed tip speed and inlet conditions, variations in rotor total pressure rise will be reflected in corresponding variations in increase in absolute outlet angle. For the test rotor, as shown in Fig. 12, total pressure rise decreases in the 90^{o} quadrant and increases in the 270^{o} quadrant. Thus, less increase in outlet angle would be expected around 90^{o} and more around 270^{o} as crossflow velocity is increased. This variation in increase in outlet angle is about 180^{o} out of phase with the variation in inlet angle shown in the lower part of Fig. 13.

Thus, the magnitude of the net circumferential variation of rotor outlet angle with crossflow velocity should be somewhat less than the value for rotor inlet angle.

The circumferential variation of flow angle at the rotor outlet (upper part of fig. 13) represents a distortion of the free-stream flow entering the stator. If the stator is designed for minimum-loss setting angle for the static case (no crossflow), then excursions in inlet angle represent departures from minimum-loss incidence angle. Local increases in total pressure loss can then occur across the stator, depending upon the basic loss characteristics of the blade elements of the stator. In general, high stator design blade loading (i.e., diffusion factor) and high inlet Mach number will produce small incidence-angle range and a larger average loss in total pressure across the stator during crossflow.

Stage Exit

Circumferential variations in total pressure and flow angle measured at mid-radius at the duct exit are shown in Fig. 14. The flow variations in crossflow observed at the rotor exit are seen to persist through to the exit of the duct. Of particular importance is the large decrease in minimum total pressure compared to the relatively small increase in maximum pressure, as in the case of the rotor outlet (fig. 12).

The reduced level of total pressure at the duct outlet compared to the rotor outlet at mid-radius (figs. 12 and 14), is not necessarily a direct reflection of the inlet-angle distortion effect on the losses across the stator blade elements. The rotor blades contained damper wires, and the loss associated with the dissipation of the wakes from these wires may be affecting the total pressure readings at the mid-radius point at the duct exit.

On the basis of the above discussion of the internal flow distributions in the model lift fan tested, it appears that circumferential distortion of the inlet free-stream flow is a much stronger contributor to the reduction in stage outlet total pressure in crossflow than flow separation in the inlet bellmouth.

FAN BACK PRESSURE

The fan stage was designed with the assumption that the static pressure at the exit of the duct would be equal to the ambient pressure. However, this was not found to be the case. With exit louvers off, fan duct exit static pressure was found to decrease with both increasing rotor tip speed and increasing crossflow velocity. With louvers on, the duct-exit static pressure tended to increase as louver deflection angle was increased. Thus, the fan experienced a wide variation in back pressure over the test range of operation. An indication of the nature and magnitude of the back pressure variations will be given in the next series of figures.

The variation in local static pressure ratio at various locations in the exit of the fan assembly under static conditions without exit louvers is shown in Fig. 15 as a function of rotor corrected tip speed. Static pressures were measured on the walls of the fan duct near the exit, on the base surface between the fan and the turbine flow passages, and on the base surface of the turbine. The figure reveals below ambient pressures throughout, with exit pressures decreasing from the outer surface of the fan passage to the center of the turbine base. The reduced turbine base pressure is not unexpected since it is known from previous model tests of short nozzles (e.g., refs. 39 and 40) that an axial discharge would tend to produce below-ambient base pressures.

The effect of crossflow velocity and louver position on fan duct exit pressure is illustrated in Fig. 16. Variations are presented for the average of the hub and tip static pressure values for several louver angles at design tip speed. Values for the case with louvers off are also included, as shown by the dashed curve. The expected increase in duct exit static pressure is observed as louver deflection angle is increased. However, increasing crossflow velocity produces a decrease in duct exit static pressure for all louver configurations. This latter trend is interpreted as indicating some form of interaction effect between the discharge streams from the fan and the crossflow airstream.

In an attempt to investigate the reasons for the backpressure variations found under static conditions, plots were made of the variation in exit-axial

velocity and exit flow angle for both the fan and turbine exhausts, as shown in Fig. 17. First, fan duct flow angle, β_e, was very nearly axial, so that the indicated radial difference in fan duct static pressure (fig. 15) cannot be attributed to residual tangential velocity. The relatively large flow angle in the exit flow from the turbine could generate a measurable radial static pressure gradient across the turbine flow passage. However, the observed variations in fan base and turbine base pressures in Fig. 15 do not appear to be completely consistent with the variation in turbine exit flow angle in Fig. 17.

It was conjectured that a more logical cause of the reduced fan exit static pressure was the propagation of the low turbine base pressure into the fan flow. As shown in Fig. 17, the calculated turbine exit axial velocity was around 30 percent greater than the calculated fan duct exit velocity. Such high values of turbine discharge velocity will produce relatively low base pressures and will tend to aspirate the fan exit flow. This interpretation was explored by installing a 6-in.-long cylindrical separator between the fan and turbine discharge flows as shown in the photograph of Fig. 18. Tests then revealed, as demonstrated in Fig. 19, that the separation of the fan and turbine discharge flows did indeed result in an increase in the fan exit static pressure. However, the decrease in fan exit static pressure with increasing crossflow velocity persisted. This further verifies the suspicion of a discharge flow/crossflow interaction effect on fan base pressure.

In view of the rather sizeable variation in fan exit back pressure over the test range of variables, it is well to question the possible effect of these back pressure variations on fan operating point, and to check into the possible contribution of back pressure effects to the variation of fan gross thrust in crossflow as observed in Fig. 4.

PERFORMANCE MAPS

In order to evaluate the relative effects of inlet flow distortion and exit back pressure on fan performance in crossflow, it was helpful to define the basic performance map of the fan stage.

Static Case

A fan stage performance map without crossflow was obtained by attaching a throttling device to the rear surface of the fan as shown in Fig. 20. The throttle was designed to achieve a variation in ratio of duct-exit static pressure to ambient pressure from 0.9 to 1.15. The outer member of the throttle contained a diffusing section to achieve the lower values of exit static pressure. A conical throttle plug was supported by a cylindrical member which was fastened to the hub section of the fan. The cylinder separated the turbine and fan exhausts. The throttle plug was remotely positioned by the actuator as shown in the figure.

A conventional stage performance map was obtained for the model lift fan as shown in Fig. 21. The design point of the fan was pressure ratio of 1.28 and specific weight flow of 31.5 lb/sec/ft^2. Also shown on the figure are lines of constant duct exit static pressure ratio. The solid symbols denote data obtained from the use of the exit louvers as a throttle. Trends of variation were similar for both throttle methods, although the average total pressure ratio was always higher with the use of louvers. The data points shown were all within the stable operating range of the fan stage. Choking occurred at 90, 100, and 110 percent of design speed. At design speed, a reduction in back pressure below ambient will move the operating point into the choked region.

From the standpoint of the aircraft application, the most important propulsion parameters are fan thrust and input power. Consequently, the static performance map was redefined in terms of fan thrust (function of flow rate and total pressure ratio) and fan power input. These maps are shown in Figs. 22 and 23, respectively. The duct exit static pressure ratio was chosen as the independent variable because it provides a direct assessment of the fan back pressure. The static performance maps of Figs. 22 and 23 show the data obtained using the exit louvers as well as the throttle plug.

The maps of Figs. 22 and 23 clearly show the overall effect of fan back-pressure variations of fan static gross thrust and power input. At design tip speed, a reduction in duct-exit static pressure below ambient (louvers-off case, fig. 15) resulted in a reduction in fan gross thrust compared to the design value ($p_e/p_o = 1.0$). This reduction in thrust was a result of fan operation in the choked region. Thrust vectoring with louvers tends to first increase and

then decrease thrust. At lower levels of tip speed, fan gross thrust tends to decrease as back pressure is increased for all values of louver position.

Crossflow Case

The fan thrust performance map and the fan power input map will now be used to analyze the effects of crossflow on fan performance.

A fan thrust map in crossflow was determined as shown in Fig. 24 for the test conditions of design tip speed and zero wing angle of attack. The upper curve is the variation in thrust obtained for the static case (no crossflow) as shown in Fig. 22. Locations corresponding to the various louver positions are given on this curve. Corresponding thrust/exit pressure curves were then constructed from the data obtained over a range of crossflow velocities. These data points were obtained by varying the exit louver position and also by removing the louvers. The crossflow curves appear to be similar in form to the static thrust variation. Curves of constant louver position can then also be identified, as shown by the dashed lines.

The relative effects of back pressure and inflow distortion on fan gross thrust can now be readily determined from the variations of Fig. 24. The basic effect of inflow distortion (inlet boundary layer separation and total pressure losses across rotor and stator) is taken as the change in gross thrust with crossflow velocity at a fixed value of duct exit static pressure ratio. For example, at $p_e/p_o = 1.0$, an approximately 10 percent reduction in fan gross thrust is indicated due to inflow distortion when crossflow velocity is increased from 0 to 240 ft/sec.

For the particular fan configuration tested, crossflow tends to both increase inflow distortion and decrease back pressure, so that the net effect on thrust at a given tip speed is that obtained by moving along a line of constant geometric configuration (i.e., louver position, angle of attack). Corresponding crossflow maps for fan power input can also be established, as illustrated in Fig. 25. The necessary fan performance characteristics in crossflow can then be determined from these performance maps.

Finally, since a lift fan is likely to be required to operate over a range of tip speeds, a gross thrust envelope map can be established as illustrated in

Fig. 26. As indicated previously in Fig. 4, fan gross thrust characteristics are likely to be different for different tip speed levels. For example, at 70 percent speed, according to the static thrust performance map of Fig. 22, a reduction in back pressure below ambient with louvers off will result in a slight increase in gross thrust. This trend, in conjunction with an apparent reduced inflow distortion effect, resulted in a small net increase in fan gross thrust in crossflow as found in Fig. 26. Comparable thrust envelope plots could then be established for other wing angle of attack positions.

SUMMARY AND CONCLUDING REMARKS

Wind tunnel tests of a wing-installed model lift fan with coaxial drive turbine revealed a decrease in fan gross thrust of the order of 12 percent at design tip speed as crossflow velocity was increased to 240 ft/sec (164 mph). Crossflow thrust losses at lower tip speeds were smaller in magnitude. Although the crossflow thrust loss was not very large, there was a substantial deviation of measured fan thrust from the ideal value, which increased with crossflow velocity.

Fan thrust variations in crossflow were found to be the result of the effects of inflow distortion and back pressure variations induced by the crossflow. Inflow distortion affected fan performance by two mechanisms: (1) reduced weight flow and inlet total pressure arising from local separation of the boundary layer on the forward part of the inlet bellmouth; and (2) by losses in total pressure across the rotor and stator blade rows arising from circumferential variations in inlet flow angle. For the bellmouth design of the model fan tested, inlet flow separation did not appear to be a serious factor in thrust decline.

Fan back pressure (fan duct exit static pressure) was found to decrease with increasing rotor tip speed and increasing crossflow velocity, and to increase with increasing vectoring louver angle. Fan back pressure decrease with tip speed was established to be the result of the turbine base pressure effect. Fan back pressure decrease with crossflow was conjectured to be the result of some interaction effect between the fan assembly discharge streams and the crossflow stream. The overall effect of back pressure variations depends on the fan stage design point and operating range.

It should be possible to reduce fan back pressure effects by appropriate design of the fan and turbine exit duct geometry according to short-nozzle technology (i.e., direct discharge flows toward the axis of the fan and use concave turbine base surfaces of minimum area). It is also likely that fan designs in which the drive turbine exhaust is outside the fan stream (i.e., tip-turbine driven lift fans) will exhibit smaller back-pressure variations than fans with high-velocity turbine exhaust on the inside of the fan stream (integral turbine lift fan).

Overall fan performance in crossflow can readily be established from plots of fan gross thrust and power input against back pressure ratio for constant tip speed over the range of crossflows and orientations of interest.

The overall significance of these results with respect to lift fan technology development is considered to be twofold. First, the data obtained herein appear to point to three major ingredients that determine fan crossflow performance; namely: inflow distortion; basic stage performance characteristics; and back pressure. Theoretical and experimental research in these three areas may lead to methods for synthesizing overall fan behavior in crossflow, so that fan performance can be predicted for a given design and installation. Such activities are currently being pursued at the NASA Lewis Research Center. Secondly, this preliminary insight into the detailed behavior of a lift fan in crossflow may lead hopefully to means for improving fan design and response characteristics.

REFERENCES

1. Anon.: "Conference on V/STOL and STOL Aircraft," SP-116, 1966, NASA, Washington D.C., pp. 311-407.

2. Jagger, D. H. and Kemp, E. D. G., "The Potential and Development of a V/STOL Inter-City Airliner," Aircraft Engineering, Vol. 42, No. 1, Jan. 1970, pp. 6-13.

3. Deckert, W. H. and Hickey, D. H., "Summary and Analysis of Feasibility Study Designs of V/STOL Transport Aircraft," Journal of Aircraft, Vol. 7, No. 1, Jan-Feb. 1970, pp. 66-72.

4. Brown, D. G., "The Case for V/STOL Aircraft in Short Haul Transportation," Paper 700333, Apr. 1970, SAE, New York, N. Y.

5. Novak, L. R., "A Low-Risk Approach to Development of a Quiet V/STOL Transport Aircraft," Paper 70-1409, Oct. 1970, AIAA, New York, N. Y.

6. Hill, J. G., "An All Turbofan VTOL or STOL Intercity Transport," Journal of Aircraft, Vol. 8, No. 4, Apr. 1971, pp. 254-258.

7. Hickey, D. H. and Hall, L. P., "Aerodynamic Characteristics of a Large-Scale Model with Two High Disk-Loading Fans Mounted in the Wing," TN D-1650, 1963, NASA, Moffett Field, Calif.

8. Kirk, J. V., Hickey, D. H., and Hall, L. P., "Aerodynamic Characteristics of a Full-Scale Fan-in-Wing Model Including Results in Ground Effect with Nose-Fan Pitch Control," TN D-2368, 1964, NASA, Moffett Field, Calif.

9. Hall, L. P., Hickey, D. H., and Kirk, J. V., "Aerodynamic Characteristics of a Large-Scale V/STOL Transport Model with Lift and Lift-Cruise Fans," TN D-4092, 1967, NASA, Moffett Field, Calif.

10. Kirk, J. V., Hodder, B. K., and Hall, L. P., "Large-Scale Wind-Tunnel Investigation of a V/STOL Transport Model with Wing-Mounted Lift Fans and Fuselage-Mounted Lift-Cruise Engines for Propulsion," TN D-4233, 1967, NASA, Moffett Field, Calif.

11. Hall, L. P., Hickey, D. H., and Kirk, J. V., "Aerodynamic Characteristics of a Large-Scale V/STOL Transport Model with Lift and Lift-Cruise Fans," TN D-4092, 1967, NASA, Moffett Field, Calif.

12. Newsom, W. A., Jr., "Wind-Tunnel Investigation of a V/STOL Transport Model with Four Pod-Mounted Lift Fans," TN D-5942, 1970, NASA, Hampton, Va.

13. Newsom, W. A., Jr. and Moore, F. L., "Wind-Tunnel Investigation of a V/STOL Transport Model with Six Wing-Mounted Lift Fans," TN D-5695, 1970, NASA, Hampton, Va.

14. Lieblein, S., "A Review of Lift Fan Propulsion Systems for Civil VTOL Transports," Paper 70-670, June 1970, AIAA, New York, N.Y.

15. Lieblein, S., "Problem Areas for Lift Fan Propulsion for Civil VTOL Transports," presented at DGLR (Deutsche Gesellschaft für Luft-und Raumfahrt), Symposium on VTOL Propulsion, Münich, Germany, Oct. 1970.

16. Grahame, W. E., "Aerodynamic Effects of Lift-Jet and Lift-Fan Inlets in Transition Flight," Journal of Aircraft, Vol. 6, No. 2, Mar.-Apr. 1969, pp. 150-155.

17. Shumpert, P. K. and Harris, A. E., "Full-Scale Development of Lift Engine Inlets for the XV-4B Aircraft," Journal of Aircraft, Vol. 6, No. 4, July-Aug. 1969, pp. 299-306.

18. Tyler, R. A. and Williamson, R. G., "Pressure Loss and Flow Distortion Measurements on Circular Compressor Intakes in Inclined Flow," LR-401, Apr. 1964, National Research Council of Canada, Division of Mech. Engr., Ottawa, Canada.

19. Tyler, R. A. and Williamson, R. G., "An Experimental Investigation of Inclined Compressor Inflow," Canadian Aeronautics and Space Journal, Vol. 12, No. 2, Feb. 1966, pp. 45-62.

20. Tyson, B. I., "Tests of Air Inlets for Jet Lift Engines," Paper 860B, Apr. 1964, SAE, New York, N.Y.

21. Schaub, U. W., Bassett, R. W., and Cockshutt, E. P., "An Investigation of the Aerodynamics of Intakes in the Upper Surface of a Wing," Canada, National Research Council, Division of Mechanical Engineering and National Aeronautics Establishment Quarterly Bulletin, No. 4, 1966, pp. 69-99.

22. Schaub, U. W., "Experimental Investigation of Flow Distortion in Fan-in-Wing Inlets," Journal of Aircraft, Vol. 5, No. 5, Sept.-Oct. 1968, pp. 473-478.

23. Schaub, U. W., "Fan-in-Wing Aerodynamics: Experimental Assessment of Several Inlet Geometries," Paper 67-746, Oct. 1967, AIAA, New York, N.Y.

24. Schaub, U. W. and Cockshutt, E. P., "Analytical and Experimental Studies of Normal Inlets with Special Reference to Fan-in-Wing VTOL Powerplants," Proceedings of the 4th International Council of the Aeronautical Sciences Congress, R. R. Dexter, ed., Spartan Brooks, Inc., 1965, pp. 519-553.

25. Tyson, B. I., "Tests of Establish Flow Distortion Criteria for Lift Engines," Paper 64-608, Aug. 1964, AIAA, New York, N.Y.

26. Wiles, W. F., "Jet Lift Intakes," AGARDograph 103, Aerodynamics of Powerplant Installation, Part II, 1965, pp. 559-586.

27. Turner, R. C. and Sparkes, D. W., "Tests on a Simulated Lifting Fan System with Inlet Crossflow," ARC R&M-3461, 1967, Aeronautical Research Council, Great Britain.

28. Gregory, N., Raymer, W. G., and Love, E. M., "The Effect of Forward Speed on the Inlet Flow Distribution and Performance of a Lifting Fan Installed in a Wing," ARC R&M-3388, 1965, Aeronautical Research Council, Great Britain.

29. Gregory, N. and Love, E. M., "Wind Tunnel Tests on a Nacelle Fitted with Two Lifting Fans in Tandem," ARC R&M-3494, 1963, Aeronautical Research Council, Great Britain.

30. Hackett, J. E., "Wind Tunnel Tests on a Streamlined Fan-Lift Nacelle," ARC R&M-3470, 1967, Aeronautical Research Council, Great Britain.

31. Anon., "Results of Wind Tunnel Tests of a Full-Scale, Wing-Mounted, Tip-Turbine-Driven Lift Fan," TRECOM-TR-63-21, AD-426785, Sept. 1963, General Electric Co., Cincinnati, Ohio.

32. Przedpelski, Z. J., "Lift Fan Technology Studies," CR-761, 1967, NASA, Washington, D. C.

33. Stockman, N. O., "Potential Flow Solutions for Inlets of VTOL Lift Fans and Engines," Analytic Methods in Aircraft Aerodynamics, SP-228, 1970, NASA, Washington, D. C., pp. 659-681.

34. Yuska, J. A., Diedrich, J. H., and Clough, N., "Description of the 9-Foot-By-15-Foot V/STOL Wind Tunnel at the Lewis Research Center," Technical Memorandum (to be published) NASA, Cleveland, Ohio.

35. Stockman, N. O. and Lieblein, S., "Theoretical Analysis of Flow in VTOL Lift Fan Inlets Without Crossflow," TN D-5065, 1969, NASA, Cleveland, Ohio.

36. Johnsen, I. A. and Bullock, R. O., "Aerodynamic Design of Axial-Flow Compressors," SP-36, 1965, NASA, Washington, D. C.

37. Moffitt, T. P., "Design and Experimental Investigation of a Single-Stage Turbine with a Rotor Entering Relative Mach Number of 2," RM E58F20a, 1958, NACA, Cleveland, Ohio.

38. Moffitt, T. P. and Klag, F. W., Jr., "Experimental Investigation of Partial- and Full-Admission Characteristics of a Two-Stage Velocity-Compounded Turbine," TM X-410, 1960, NASA, Cleveland, Ohio.

39. Baker, V. D., Johnson, R. A., Brasket, R. G., and Lamb, O. P., "Experimental Results with Lift Engine Exhaust Nozzles," Paper 65-574, June 1965, AIAA, New York, N.Y.

40. Kentfield, J. A. C., "Nozzles for Jet-Lift V/STOL Aircraft," Journal of Aircraft, Vol. 4, No. 4, July-Aug. 1967, pp. 283-291.

E-6359

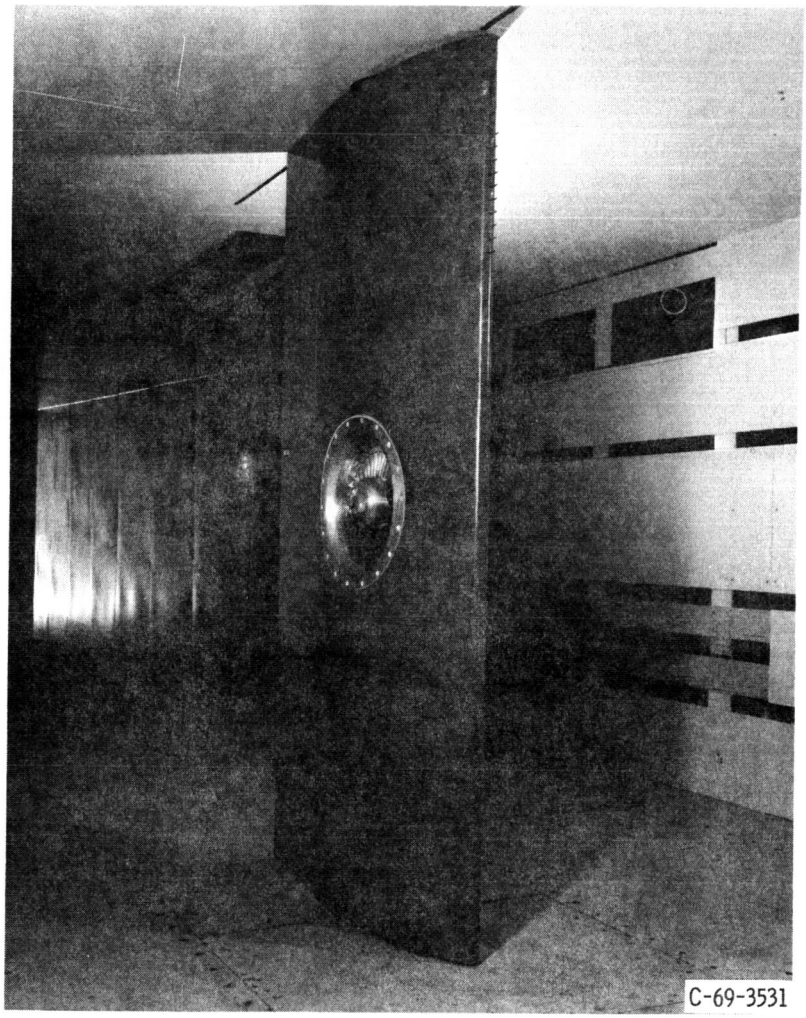

Figure 1. - Fifteen-inch diameter fan-in-wing model installed in the Lewis Research Center 9- by 15-Foot V/STOL test section.

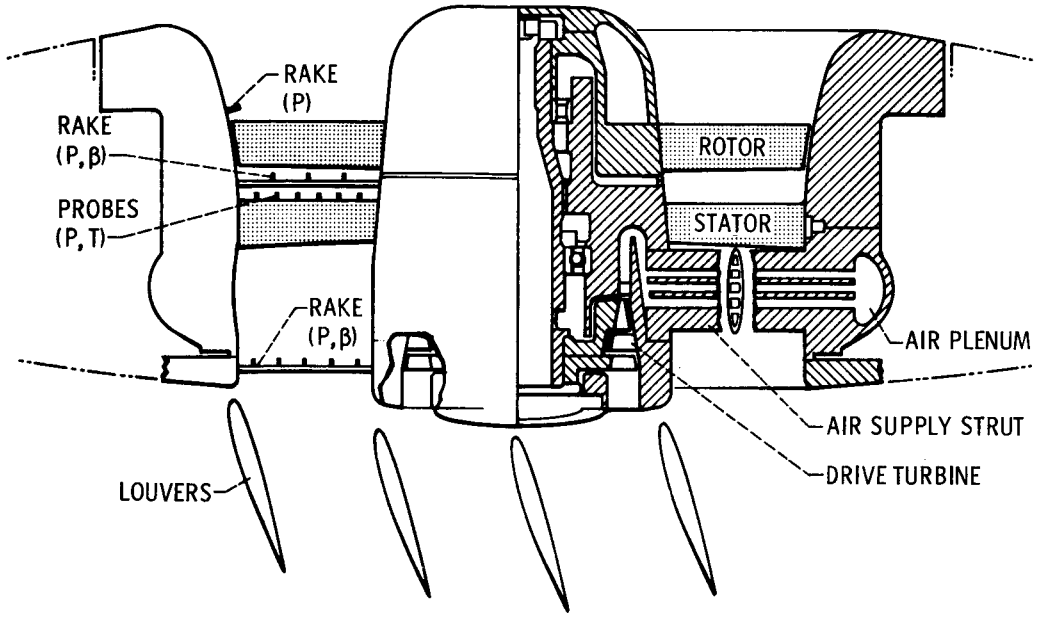

Figure 2. - Cross section of 15-inch model lift fan.

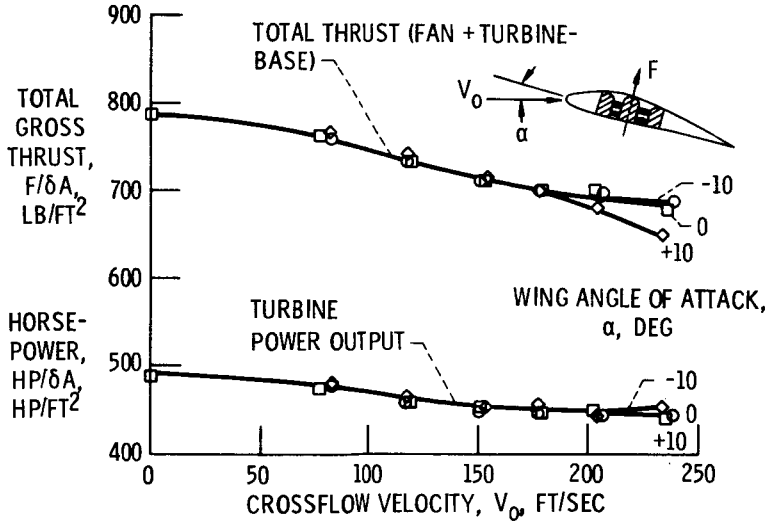

Figure 3. - Overall performance of fan assembly in crossflow. Louvers off; design tip speed, 980 ft/sec.

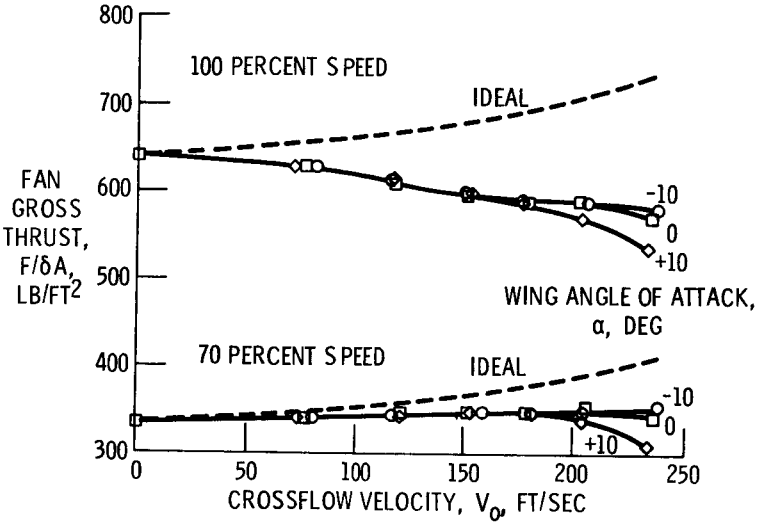

Figure 4. - Gross thrust of fan stage in crossflow. Louvers off.

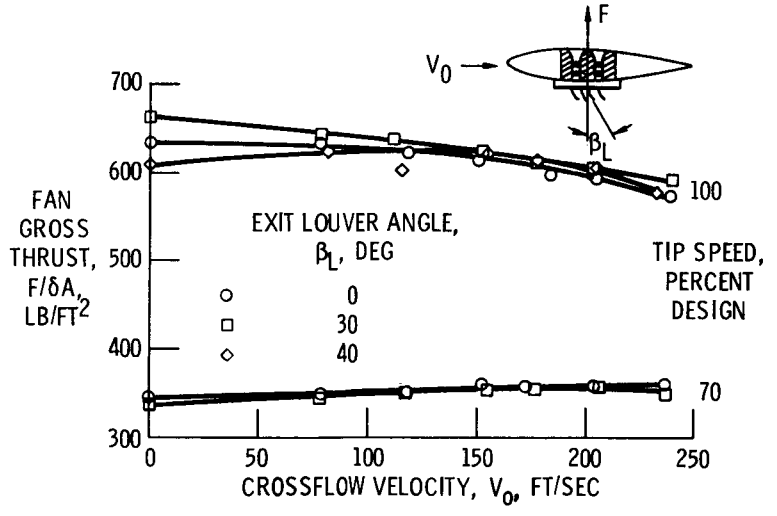

Figure 5. - Gross thrust of fan stage with exit louvers on wing. Zero wing angle of attack.

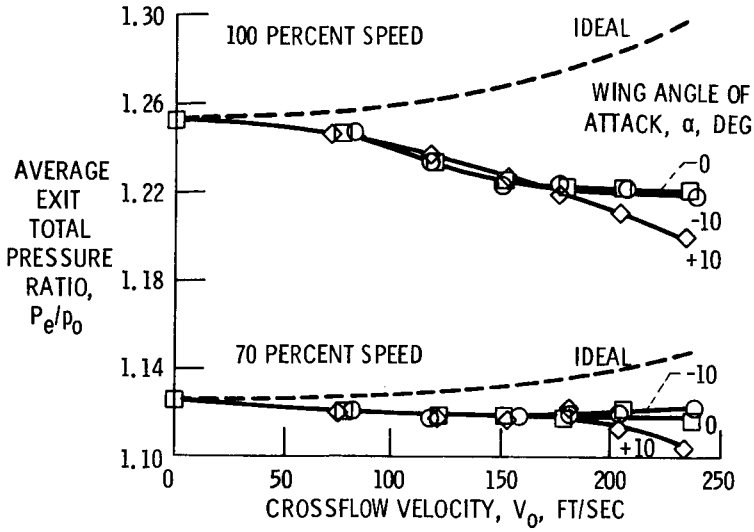

Figure 6. - Fan duct exit total pressure. Louvers off.

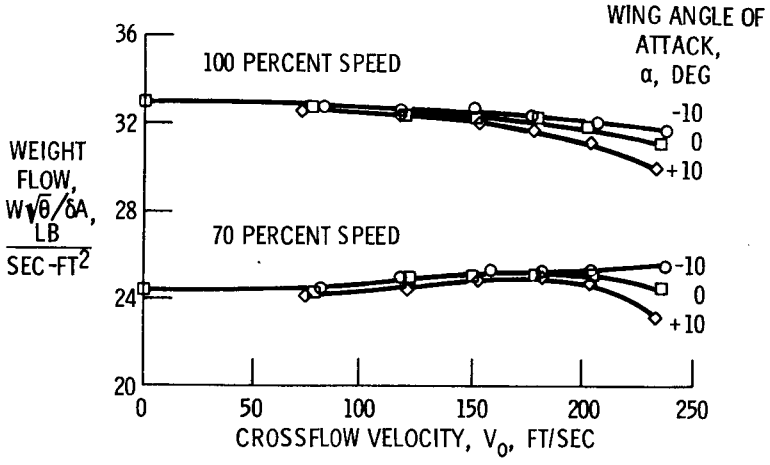

Figure 7. - Fan flow rate. Louvers off.

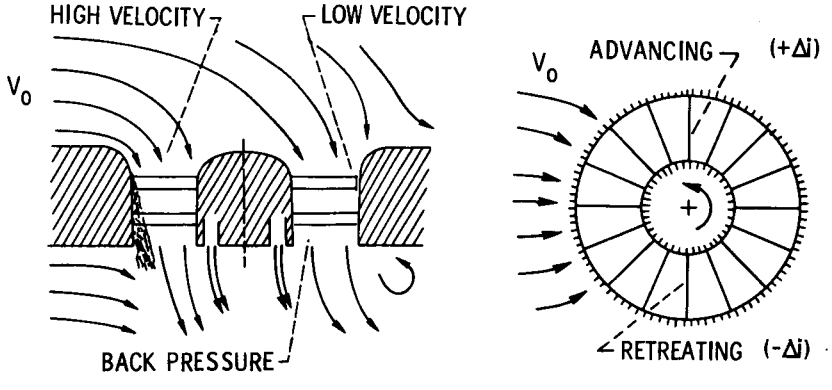

(A) EFFECT ON THROUGHFLOW VELOCITY.

(B) EFFECT ON ROTOR INCIDENCE ANGLE.

CS-56232

Figure 8. - Lift fan inflow in crossflow.

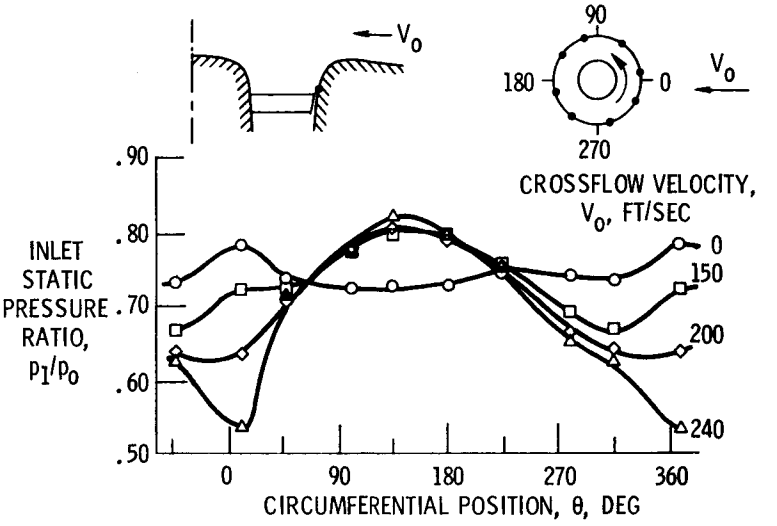

Figure 9. - Static pressure on bellmouth at rotor inlet. Design tip speed; zero angle of attack.

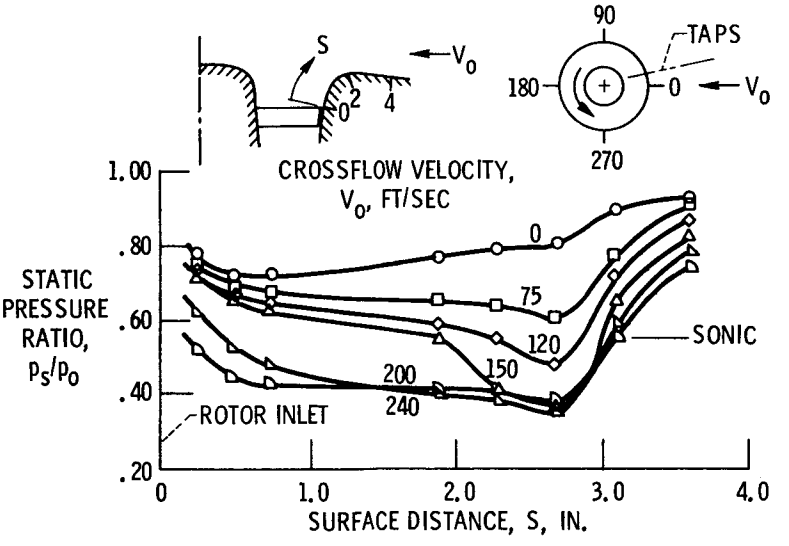

Figure 10. - Pressure variation on bellmouth surface. 10 Degree position; zero angle of attack.

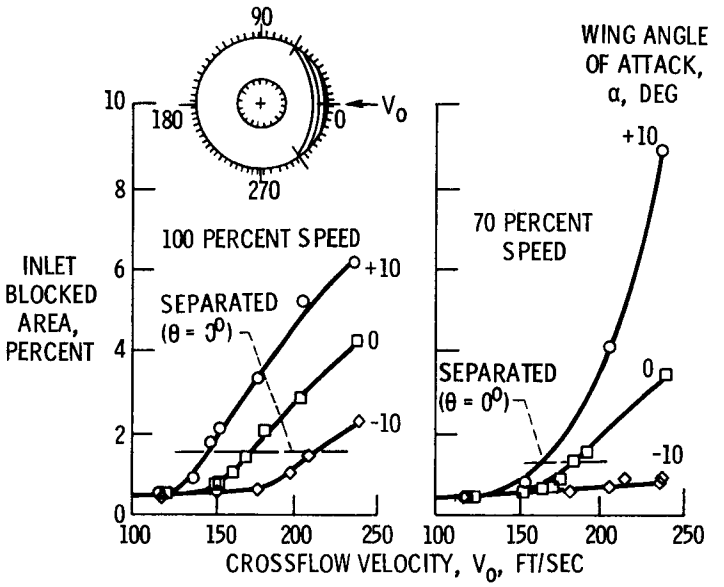

Figure 11. - Rotor inlet-area blockage due to bellmouth surface boundary layer.

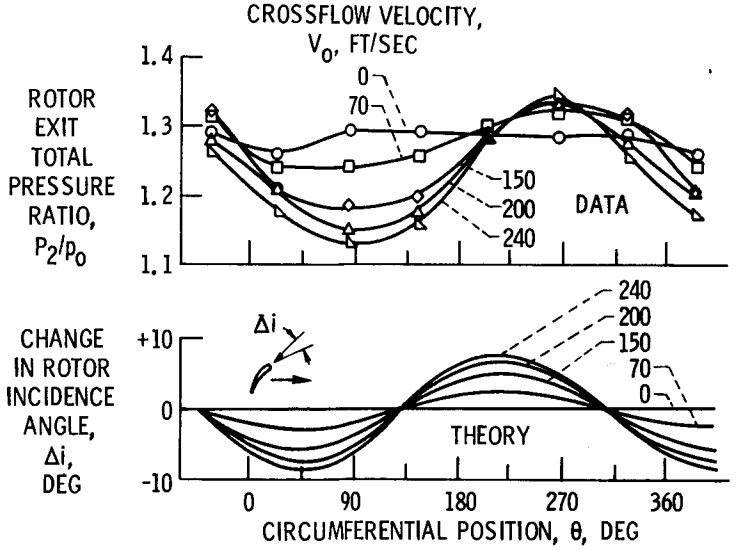

Figure 12. - Rotor outlet total pressure in crossflow. Mid-passage radius; design tip speed.

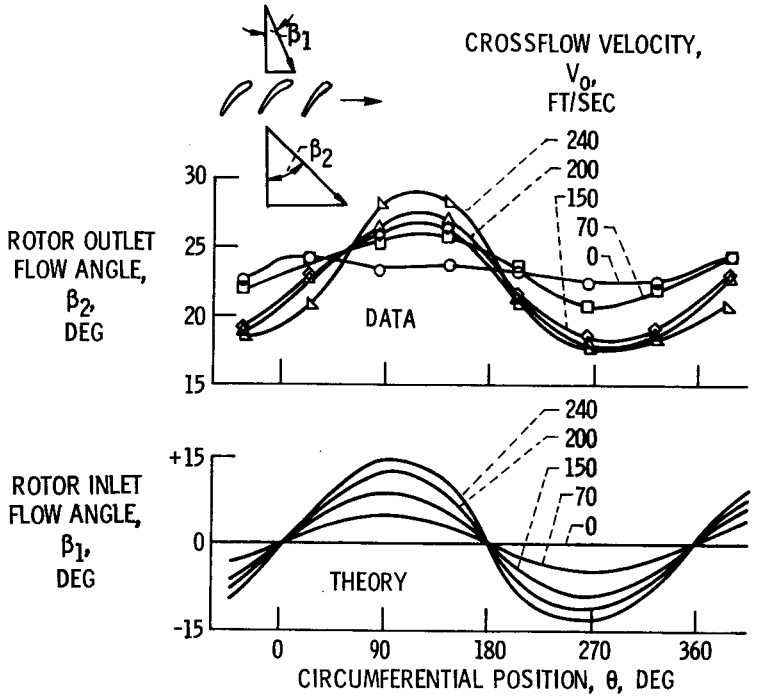

Figure 13. - Rotor flow angle in crossflow. Midpassage radius; design tip speed.

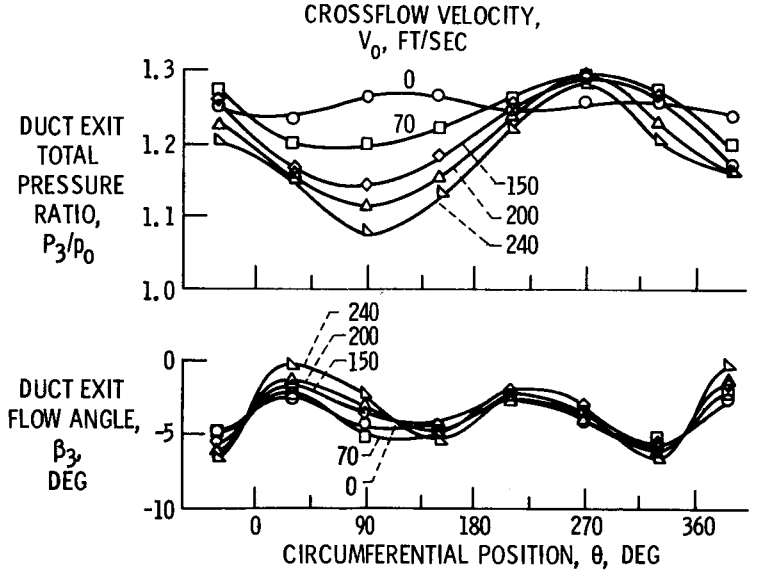

Figure 14. - Duct exit total pressure and flow angle in crossflow. Mid-passage radius; design tip speed.

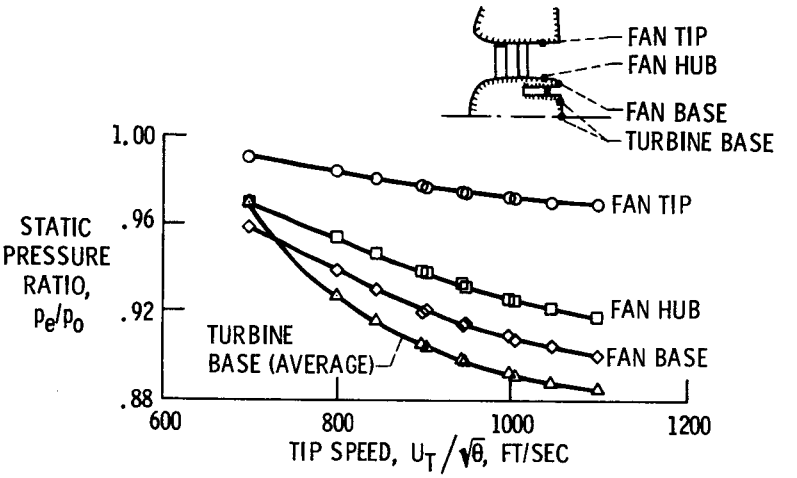

Figure 15. - Exit static pressures. Louvers off; no cross-flow.

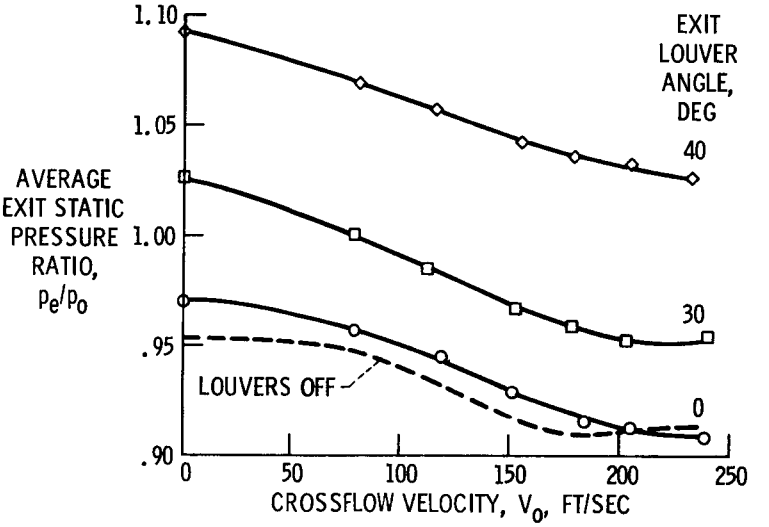

Figure 16. - Fan duct exit static pressure in crossflow. Design tip speed; zero angle of attack.

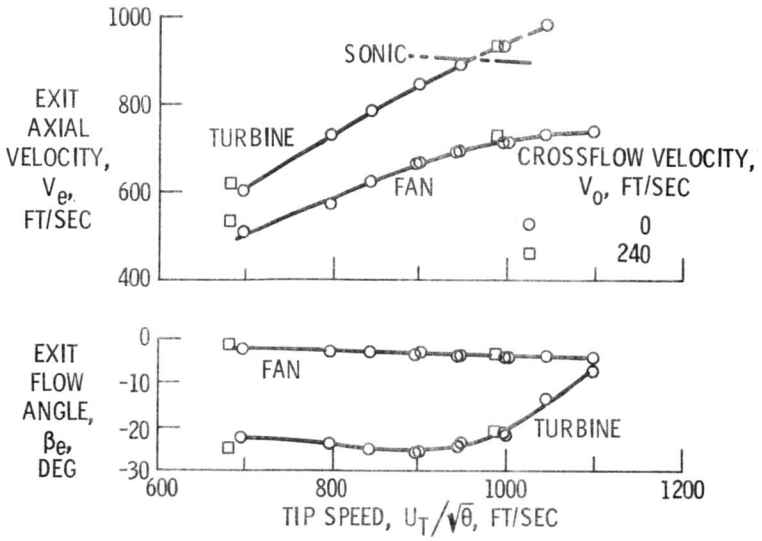

Figure 17. - Exit velocities and angles. Louvers off; zero angle of attack.

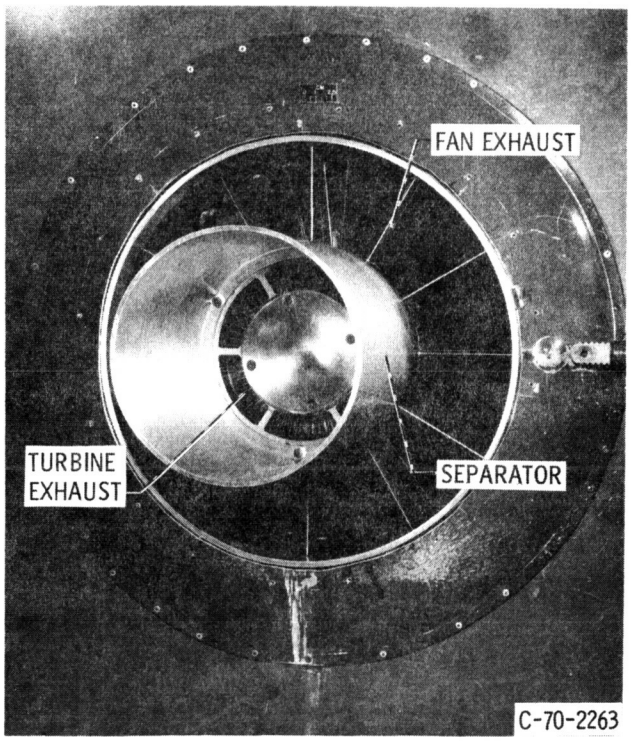

Figure 18. - Cylindrical separator between fan and turbine exhaust flows; 3.9-inch diameter by 6-inch long.

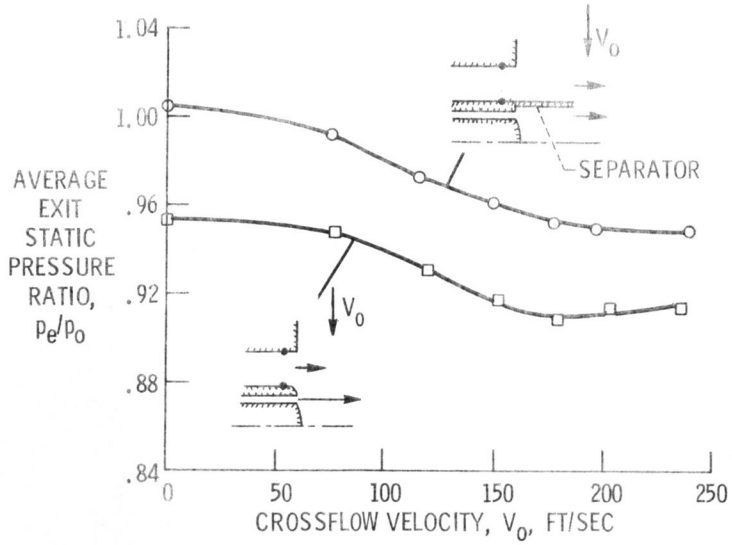

Figure 19. - Effect of fan/turbine flow separator on fan duct exit static pressure. Design tip speed; zero angle of attack.

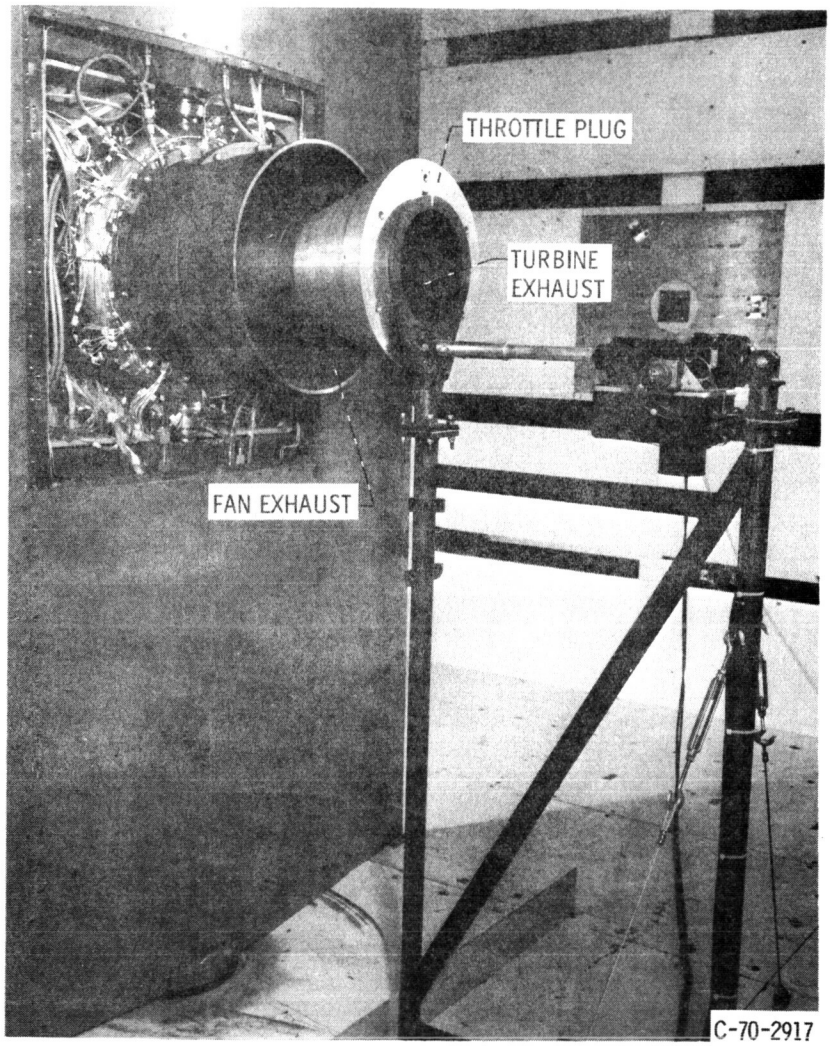

Figure 20. - Remotely actuated throttle plug for fan performance map.

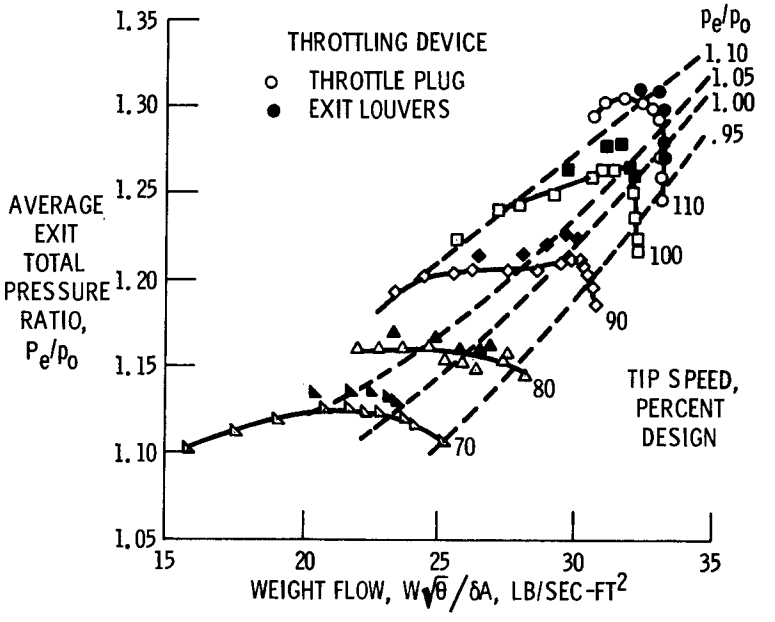

Figure 21. - Conventional stage performance map. No crossflow.

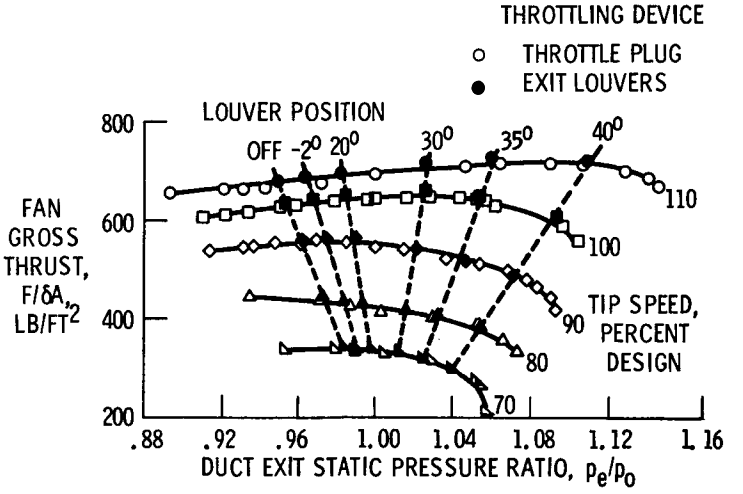

Figure 22. - Fan thrust performance map. No crossflow.

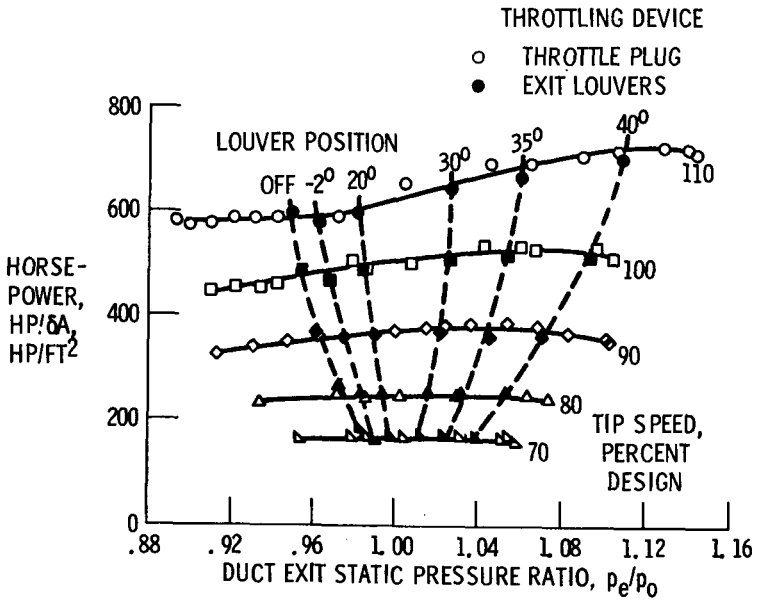

Figure 23. - Fan power input map. No crossflow.

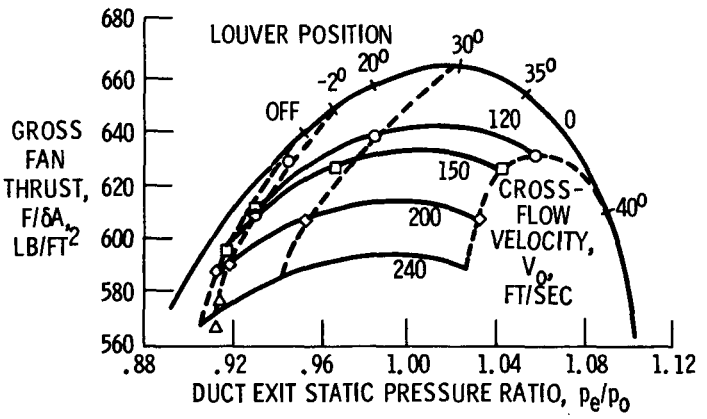

Figure 24. - Fan thrust performance map in cross-flow. Design tip speed; zero angle of attack.

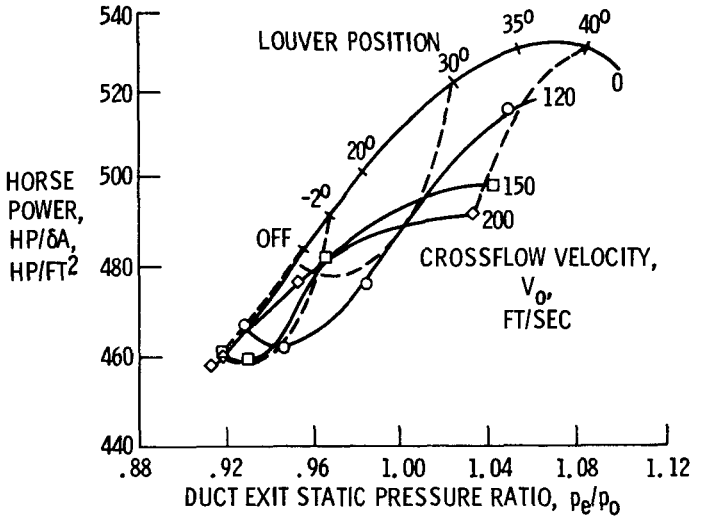

Figure 25. - Fan power map in crossflow. Design tip speed; zero angle of attack.

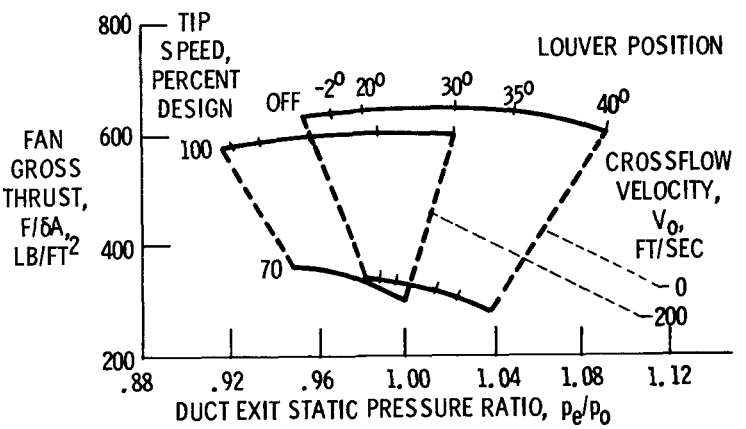

Figure 26. - Fan gross thrust envelope. Zero angle of attack.